Tomislav Senčić

Professor
University of Rijeka
Faculty of Mechanical Engineering
Croatia

Vedran Mrzljak

Assistant Professor
University of Rijeka
Faculty of Mechanical Engineering
Croatia

Ozren Bukovac

Assistant Professor
University of Rijeka
Faculty of Mechanical Engineering
Croatia

Josip Batista

Postdoctoral Researcher
University of Rijeka
Faculty of Mechanical Engineering
Croatia

Influence of Mesh and Combustion Parameters on a Spark Ignition Engine CFD Simulation

In the current paper, a CFD simulation study on a pent-roof, spark ignition engine was performed. The scope was to analyze the basic parameters that influence the performances of the simulation: mesh configuration, mesh refinement, turbulence model, and flame wrinkling model parameters. It was used as the OpenFOAM solver for spark ignition engines. The solver was modified by adding the layer addition/removal mechanism for the mesh. Further, a Zeldovich extended NOx model was implemented. Four different mesh configurations were tested with different refinement levels. A set of different turbulence models and initial parameters and different flame wrinkling model parameters were tested. It was observed how all these parameters influence the rate of heat release, cylinder pressure, temperature, the level of turbulent kinetic energy, the flame wrinkling factor, and finally the resulting concentration of nitride monoxide.

Keywords: CFD simulation, Spark Ignition Engine, simulation mesh configuration, turbulence model, flame wrinkling model, NOx emissions

1. INTRODUCTION

The internal combustion engine has been the primary power plant that provides power to our transport means for more than a century. In the last decades, envi–ronmental problems, partially related to internal com–bustion engines are gaining attention. In the first place, this is the carbon dioxide emission that is responsible for causing the greenhouse effect and the related global warming and climate change issues. Further, there are other emissions, like nitrogen oxides, unburned hydrocarbons, carbon monoxide, and particulate matter. Hence, legislation pushes ever more stringent emission limits for internal combustion engines. Some govern–ments announced the complete replacement of internal combustion engine-powered cars with other solutions, like electric or hydrogen-powered cars. However, there are still many limitations of these technologies and it seems that the internal combustion engine is going to be developed further parallel to these solutions.

Some of the combinations that are planned are hybrid systems where internal combustion engines are paired with electric motors. Other arrangements involve the use of alternative fuels which allow a lower carbon footprint, such as biofuels (bio-methanol, bio-ethanol, and biodiesel). Ammonia combustion is also in the focus as a possible, carbon-free fuel. Hydrogen combustion is also being tested in internal combustion engines, pure or blended with more conventional fuels. Another solution is the artificial synthesis of hydrocarbon fuels from captured carbon dioxide and green hydrogen known as e-fuels. In the development

process, various blends among alternative and fossil fuels are being tested. Also, alternative combustion modes are being developed such as dual fuel engines, HCCI combustion, and similar. Gas after treatment is another field that is being developed in order to reduce combustion-related problems. However, it is hard to imagine a future without the internal combustion engine, especially in the marine and commercial environment. Hence, the development of IC engines remains an important topic of scientific investigations.

Engine development is performed via experimental studies where the engine is set on a test bench with the crankshaft connected to a brake that simulates the working torque. The engine is connected to the fuel, cooling, and exhaust gas systems which ensure its operation. Many parameters are measured, such as power, torque, fuel consumption, exhaust gas tempe–rature, and composition. In-cylinder pressure is another important parameter together with components' mecha–nical and thermal stresses. Such laboratory tests are very complex and costly, but important.

A cheaper and faster alternative is the computer simulation which also gives additional insight into the IC engine's internal processes. There are various kinds of simulations, but the computational fluid dynamics (CFD) simulation can give insight into the engine cy–linder processes, responsible for chemical reactions and pollutant formation. There are different commercial software that allows CFD analysis of engine processes. Some open-source projects offer CFD analysis. OpenFOAM is an open-source, free-of-charge, CFD collection of solvers and libraries written in C++ [1-3]. Of its availability, flexibility, and collaboration between users, it is a good platform to use to approach uncom–mon CFD problems. The core of the spark ignition engine combustion calculation is the flame speed. Amirante [4] provides simple and workable expressions, suitable for spark-ignition engine simulations, that allow

laminar flame speed calculations of some practical fuels. Flame propagation depends on the wrinkling process. Chatakonda et al. [5] proposed a new flame wrinkling model to apply to premixed flames where the turbulence scales can penetrate the flame. The model utilizes concepts of fractal geometry and Damköhler's limiting flame-speed scalings. Anetor et al. [6] perfor–med a CFD investigation of a modern, high-perfor–mance 4-valve engine with a quasi-symmetric pent-roof combustion chamber using OpenFOAM. Sendyka and Noga [7] performed a combined theoretical, experi–mental, and numerical analysis of a dual injection, pent-roof, spark ignition engine. They focused on the influence of the combination of port injection and direct injection on engine performance and emissions. Gundmalm [8] in his thesis performed a detailed CFD simulation using OpenFOAM, including the intake, compression, and combustion phases. The focus was on the investigation of the presence of an intake air tumble motion and later on the tendency to knocking phenomenon. Battistoni et al [9] simulated pure gasoline and pure ethanol combustion in a 4-valve single-cylinder SI engine. They assumed premixed combustion conditions and used detailed chemistry with the well-mixed combustion model approach. Simulation results are compared with data from optical engine expe–riments. Mashkour [10] and al. developed a 3D CFD simulation of a SI, pent-roof engine. They analyzed the influence of the equivalence ratio on cylinder pressure, temperature, heat transfer, and NOx emissions. Yin et al. [11] analyzed the combined effects of piston bowl geometry and a charge motion control valve (CMCV) on tumble flow and combustion features in GDI en–gines, using the commercial CFD software FIRE. In their paper, Mauro et al. [12] used a single-zone model and a CFD model. They were implemented for the simulation of the closed part of the cycle of a CFR en–gine in order to obtain an accurate heat release eva–luation. The local turbulent flame development is mo–deled using the G-equation, which provides a strict correlation to the laminar flame speed which, in turn, is a chemical property of the gas mixture. Kutkan et al. [13] used the Algebraic Flame Surface Wrinkling model to simulate a high-pressure, turbulent premixed Bunsen flame experiment. They compared the results obtained with OpenFOAM and Ansys Fluent to the experiment. Yoshy et al. [14] used OpenFOAM to analyze the ef–fects of the spark plug position on engine performance.

Here, an attempt to get a systematic insight into the influence of the mesh, turbulence, and combustion model parameters on calculated performance is done. The focus is on the heat release rate, cylinder pressure, and NO_x emissions. The analysis can be used as guidance for further spark ignition engine simulations.

The paper is organized as follows. In section 2, some parts of the mathematical model behind the OpenFOAM software for spark ignition engine simulation are presented: the transport equations, combustion mode–ling, turbulence modeling, and NOx calculation. In sec–tion 3, some details about the simulated engine and the calculation boundary conditions are reported. Then the results with comments follow the selection of the mesh configuration, the analysis of the number of cells, the

selection of the turbulence model and its parameters, and the influence of combustion model parameters. Fi–nally, some conclusions are derived in the final section.

2. MATHEMATICAL MODEL

2.1 Governing equations

In the paper, the CFD code OpenFOAM is used. It uses the finite volume method in order to calculate the variation of the main variables in the fluid continuum. The main governing equations are described in the following part. The global continuity equation yields

$$\frac{\partial \rho}{\partial t} + \nabla \cdot (\vec{u}\rho) = 0 \tag{1}$$

where ρ is the total mass density of the fluid, u is the gas velocity vector and t is the time.

The averaged momentum equation for the gas reads

$$\frac{\partial(\rho\vec{u})}{\partial t} + \nabla \cdot (\rho\vec{u}_i\vec{u}_j) = -\nabla p + \nabla \cdot \sigma + \\ + \rho g - \frac{2}{3}\nabla(\rho k) \tag{2}$$

where p is the gas pressure, σ is the viscous stress tensor, g is the specific body force, which is assumed to be constant.

The energy equation yields

$$\frac{\partial(\rho e)}{\partial t} + \nabla \cdot (\rho\vec{u}e) = -p\nabla \cdot \vec{u} - \\ -\nabla \cdot \vec{J} + \rho\varepsilon + \dot{Q}^c \tag{3}$$

where e is the specific internal energy, excluding the chemical energy, and J is the heat flux vector which is the sum of heat conduction and enthalpy diffusion. Q^c is the source term due to chemical heat release.

2.2 Spark ignition engine combustion modeling

There are several strategies to cope with the turbulent premixed combustion that takes place in spark ignition engines. Some of them are the Eddie Break Up [15], Thin Wrinkled Flame [16], and Flame Area Evolution [17].

The Weller flame wrinkling model implemented in OpenFOAM is based on the solution of two equations [18]. One is the transport equation for the spatial and temporal distribution of the progress variable b and the other solves the wrinkling factor Θ. The flame wrink–ling is calculated by simple algebraic equations based on flame speed correlation:

$$\Theta^*_{eq} = 1 - 0.62\sqrt{\frac{u'}{S_{ub}}}R_\eta \tag{4}$$

$$\Theta_{eq} = 1 + 2(1-b)(\Theta^*_{eq} - 1) \tag{5}$$

where Θ is the ratio of the turbulent flame velocity to laminar flame velocity, $\Theta = S_t / S_{ub}$; S_t is the turbulent flame speed, S_{ub} is the laminar flame speed, u' is the subgrid turbulence intensity, R_η is the Kolmogorov

Reynolds number. The flame front propagation is calculated by the following transport equation for the density-weighted mean reaction regress variable b:

$$\frac{\partial \rho b}{\partial t} + \nabla \cdot (\rho \vec{u} b) - \nabla \cdot \left(\frac{\mu_t}{S_{ct}} \nabla b \right) = \\ = -\rho_{ub} S_{ub} \Theta |\nabla b| \tag{6}$$

For a more detailed description of the combustion modeling [6] can be consulted.

2.3 Turbulence modeling

The most common model used to simulate the effects of turbulence in the flows is the k-ε model which solves two transport equations, one equation to solve the turbulent kinetic energy k and the other to calculate its dissipation rate, ε. A more detailed description and the physical meaning of the various terms can be found in [6]. The RNG model was developed using Re-Norma–lization Group (RNG) methods to account for the effects of smaller scales of motion [19]. In the standard k-ε model, the eddy viscosity is determined from a single turbulence length scale, so the calculated turbulent diffusion is that which occurs only at the specified scale, whereas, in reality, all scales of motion will contribute to the turbulent diffusion. The RNG approach, which is a mathematical technique that can be used to derive a turbulence model similar to the k-ε, results in a modified form of the ε equation which attempts to account for the different scales of motion through changes to the production term.

The k-ω is a similar two-equation model. Instead of ε there is the ω equation, where ω is the specific rate of dissipation of the turbulent kinetic energy into internal thermal energy [20]. The SST k-ω model is another common turbulence model implemented in OpenFOAM that can be used for internal combustion engine simulations. This is a hybrid turbulence model that combines aspects of the k-ε and k-ω models and is designed to be more accurate and robust for a wider range of flow regimes. It is often used in complex geometries or high Reynolds number flows.

2.4 NOₓ model

Among the products of the combustion in spark ignition engines, Nitrogen Oxides are one of the most harmful, and the one that can be controlled to a certain extent by engine parameters and settings. It is indicated as NO_x since nitrogen and oxygen combine in various atomic ratios, but all of them are more or less harmful to human health. If nitrogen is not present in the fuel, it comes to the reactions from the air. The quantification of the NO_x is usually done using the "Zeldovich extended mechanism" proposed by Zeldovich in 1946 [21]. It is based on three chemical reactions:

$$N_2 + O \leftrightarrow NO + N \tag{7}$$

$$N + O_2 \leftrightarrow NO + O \tag{8}$$

$$N + OH \leftrightarrow NO + H \tag{9}$$

Initially, nitrogen monoxide NO is formed during combustion in high-temperature regions (starting at about 2000 K), mostly from the nitrogen contained in the air. Afterward, some nitrogen monoxide NO will convert to nitrogen dioxide (NO_2) and nitrous oxide (N_2O). The mix of oxides of nitrogen is called NO_x.

The extended Zeldovich model was implemented in the code used for the paper. The lack of chemical species tracking of the simple combustion model used was solved by the assumption of a known concentration of relevant species in fresh air-fuel mixture and fully combusted products.

The transition from the concentrations in the fresh mixture and products was assumed as linearly propor–tional to the combustion progress variable b and local density ρ.

$$[H_2O] = (1-b) \cdot 0.13 \cdot \rho \tag{10}$$

$$[N_2] = [b \cdot (0.78 - 0.71) + 0.71] \cdot \rho \tag{11}$$

$$[O_2] = b \cdot 0.21 \cdot \rho \tag{12}$$

The concentration of the remaining species needed for the extended Zeldovich model is calculated as follows [22]:

$$[O] = 3.6 \cdot 1000 \cdot [O_2]^{0.5} e^{\frac{-31090}{T}} \cdot \frac{1}{(RT)^{0.5}} \cdot \rho \tag{13}$$

$$[OH] = 2.129 \cdot 100 \cdot T^{-0.57} \cdot e^{\frac{-4595}{T}} \cdot ([O] \cdot [H_2O])^{0.5} \cdot \rho \tag{14}$$

3. THE ENGINE

The engine used for the simulations in this article is an experimental single-cylinder, optical engine with a pent-roof combustion chamber and four valves described in [9]. The basic data about the engine are reported in Table 1. It can feature both direct injection and port fuel injection and is equipped with a camless electro-hydraulic valve lifting system that allows free control of valve timing. Optical access to the combustion chamber is possible through a 60 mm diameter quartz piston crown window.

Details about the pent-roof, retrieved from images in [9], are reported in Figure 1., with dimensions in millimeters.
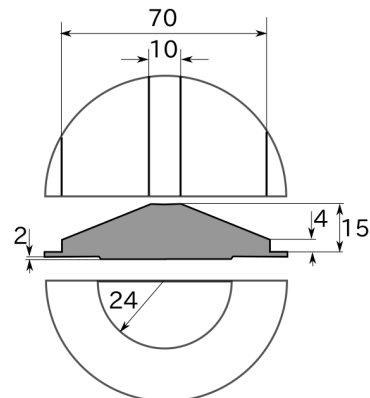

Figure 1. Engine combustion chamber

Table 1. Engine main parameters

Bore [m]	0.085
Stroke [m]	0.088
Connecting rod length [m]	0.139
Compression ratio	8.8
Engine speed [rpm]	900
Spark timing [°]	-17
Relative air-fuel ratio, λ	1.0

4. SIMULATIONS AND RESULTS

A series of simulations was performed to test the influence of the main calculation parameters like the discretization mesh type, number of cells, turbulence model and its initial values, and combustion model parameters. The validation was not carried out sepa–rately. All the simulation sets are compared to the expe–rimental result. Specifically, the measured parameter was the cylinder pressure found in [9]. The main simu–lation initial and boundary conditions are presented in Table 2.

4.1 Mesh configuration

The mesh for internal combustion engines can be complex. It includes at least a moving piston and it can include a piston bowl, a pent-roof head, and valve recesses. In order to cope with the moving piston, the layer addition/removal strategy is implemented in the engine foam solver to reduce the number of cells during the calculation and to maintain the aspect factor of the cells [23]. As the piston travels toward the TDC (Top Dead Course), layers of cells are removed, and they are added as the piston travels to the BDC (Bottom Dead Course). For some simulations, the influence of the piston and head details can be neglected. Some papers used the geometry supplied with the OpenFOAM tutorial, kivaTest like [6] and [14]. In the first part of the investigation, 4 meshes for the same engine are built with various levels of refinement in order to check how the mesh influences the basic combustion performance. The meshes at the end of the compression are represented in Figure 2, with increasing refinement from a) to d). The first mesh is a 2D mesh that does not reproduce any of the geometric details seen in Figure 1. In [24] it is shown that very simple 2D meshes can result in realistic results. The second mesh from the left is a 90° sector mesh, that represents 1/4 of the real domain, and also neglects many of the details. It is a 3D mesh with cyclic boundaries. The third mesh reproduces half of the domain with symmetry boundaries. Even if it is somewhat simplified compared to real geometry, it reproduces the basic shape of the pentroof. The last mesh is a full 3D mesh of the domain that reproduces all the minor details of the engine geometry, the pentroof, and the recession in the piston. The first three meshes were created with blockMesh, the OpenFoam basic meshes. The last one is created with Ansys ICEM CFD commercial software and then converted to OpenFOAM format. The meshes have a different number of cells. The 2D mesh has 488 cells at the beginning of the compression and, due to the layer-removing mechanism, 228 at the end of the compression. The ¼ sector mesh has from 5856 cells at the beginning to 2736 cells at the

end of the compression, the half mesh has 10560 to 4320 cells and the full mesh has 84325 to 16845 cells.

**Table 2. Simulation initial and boundary conditions**

Parameter	Value	Unit
Cylinder pressure p	70000	Pa
Gas temperature T	300	K
Piston temperature	450	K
Liner temperature	400	K
Head temperature	450	K
Velocity u	0 - 1.2	m/s
Turbulent kinetic energy k	3	m^2/s^2
Dissipation rate ε	450	m^2/s^3
Turbulent viscosity μ_t	0	kg/(ms)
Combustion regress b	1	-
Laminar flame speed Su	0.4	m/s
Flame wrinkling factor Θ	1	-
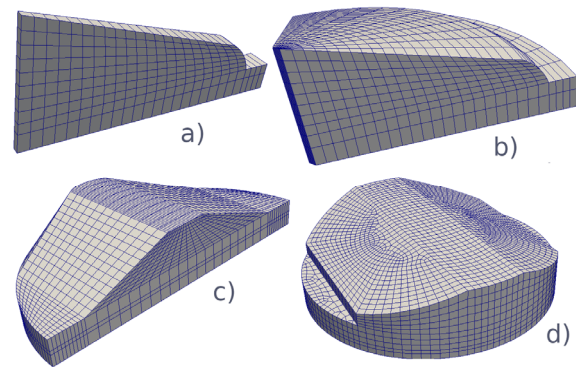
Figure 2. Investigated mesh configurations: a) 2D mesh, b) 1/4 sector mesh, c) half mesh, d) full mesh

In Figure 3. the influence of mesh configuration on the cylinder pressure is presented. It can be seen that all 4 tested configurations catch the general trend of the pressure. The pressure gradually builds up after a certain period after the ignition (at -17 ºCA). The maximum pressure obtain differs a lot, from 17 bar for the 2D mesh to 48 bar for the 1/4 sector mesh. The half-mesh and full-mesh configurations give more reaso–nable maximal pressures that are closer to the 33 bar obtained experimentally in [9]. The pressure peak of these cases comes a few degrees of crank angle too late compared to the experiment. It could be further tuned by modifying surface temperatures or by tuning the heat transfer model, but it was not the scope of the paper.
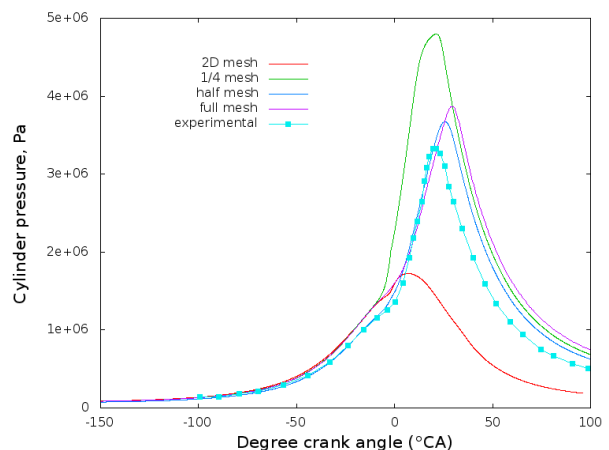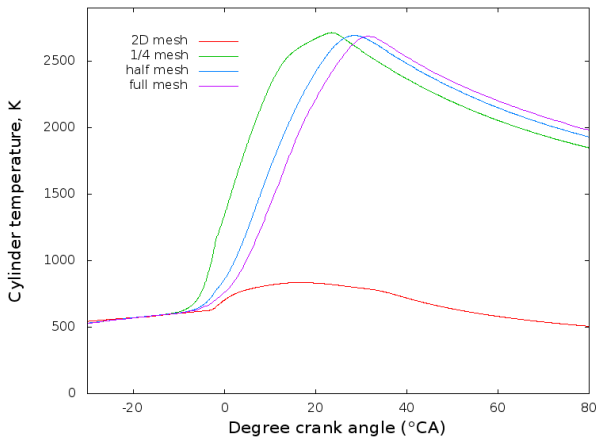

Figure 3. Mesh configuration influence on cylinder pressure

In Figure 4. the heat release rate for the different mesh configurations is shown. The heat release is intense and comes early for the 1/4 sector mesh. It comes later for the half-mesh and full-mesh confi–gurations and the heat release is more spread. For the 2D mesh, the peak comes early, but the heat release is much lower than in other cases.
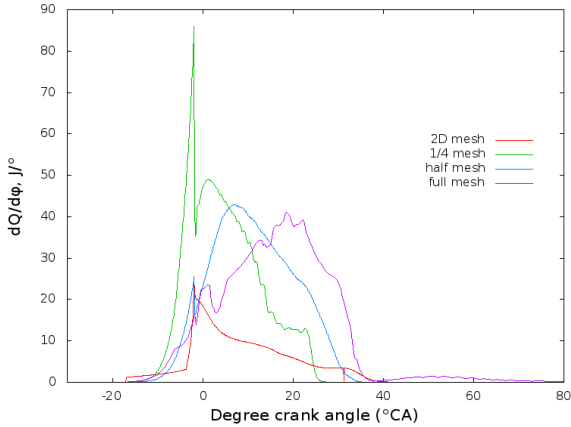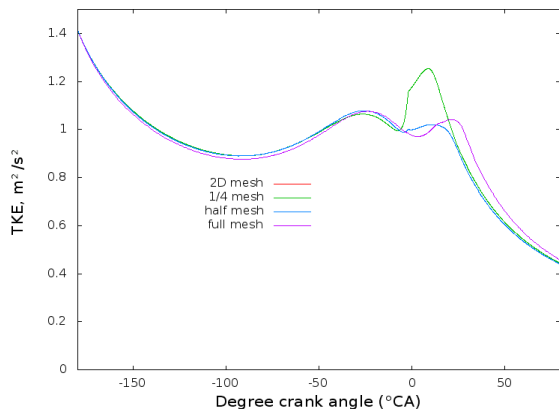

Figure 4. Mesh configuration influence on the rate of heat release

In Figure 5. the temperature for the different mesh configurations is displayed. The temperature reaches about 2700 K for all the cases, except for the 2D mesh for which the temperature reached is unrealistically low. The temperature peak is reached slightly earlier for the 1/4 sector mesh than for the other configurations.

Figure 5. Mesh configuration influence on cylinder temperature

Figure 6. Mesh configuration influence on turbulent kinetic energy

In Figure 6, the level of turbulent kinetic energy is presented. It varies from 1.4 at the beginning to 0.4 at the end of the simulated period with a characteristic trend. The case 1/4 sector mesh presents a jump of turbulent kinetic energy that follows the fast combus–tion. The case 2D mesh is not presented since its tur–bulent kinetic energy is out of the range and jumps to 15 m^2/s^2 from the beginning.

4.2 Mesh refinement

In the second set of simulations, the mesh refinement, or cell number and size was analyzed. It selected the half-mesh configuration with different cell numbers. Since the layer addition/removal function is implemented in the code, the initial number of cells is reduced as compression is going on. The number of the cells in the meshes was, for the first, coarse mesh, from 5120 at the beginning (BDC) to 1920 cells at TDC, for the second, intermediate mesh it was from 15060 to 5220 cells and for the third, finest mesh it was from 31110 to 11730 cells. In the following figures, the influence of the number of cells on the results is presented. The meshes are named on the initial number of cells.

In Figure 7. it can be seen that the maximal cylinder pressure is higher for the coarser mesh and the pressure rise starts earlier. The cylinder pressure reaches 35 bar, which is slightly more than in the experimental case. In the same case, the pressure peak is reached a few crank angles later than in the experimental case. The reason behind the pressure curves can be seen in the next figure.
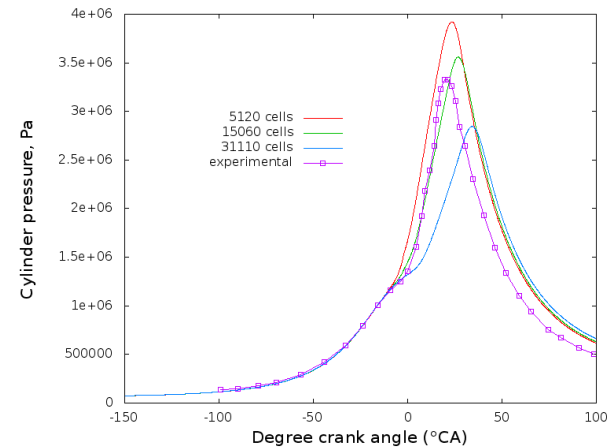
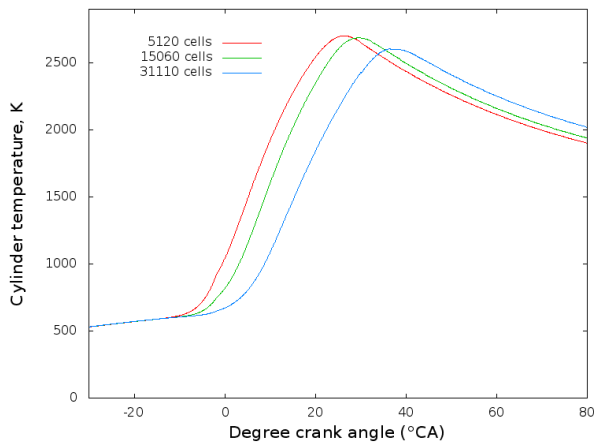**Figure 7. The number of cells influences cylinder pressure**

In Figure 8. the heat release over the crank angle is presented. It can be seen that the coarser mesh gives origin to earlier combustion with a faster reach of the peak in heat release. For the other, finer meshes, the heat release starts later and is more gradual. The heat release is reflected in the cylinder pressure and in the cylinder temperature.

As can be seen in Figure 9. the temperatures are slightly higher in the early phase for the coarser mesh, while the temperatures are lower in the later phase. In Figure 10., the influence of cell size on the turbulent kinetic energy is shown. It can be seen that the influence is very weak, but generally smaller cells result in smaller Turbulent Kinetic Energy.
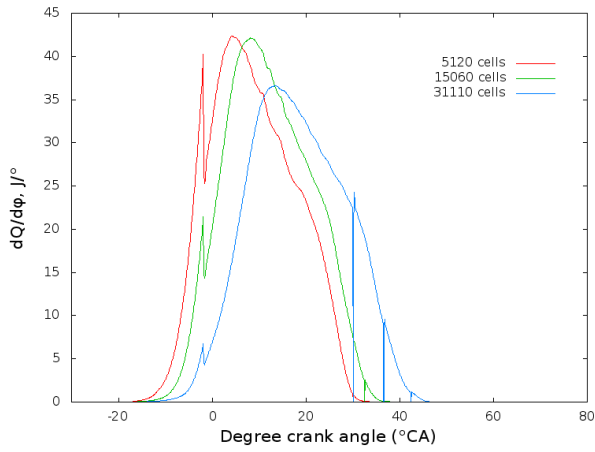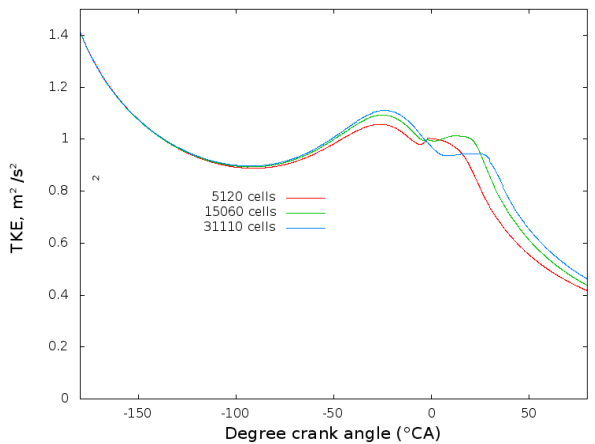
Figure 8. The number of cells influences the rate of heat release

In Figure 11., the influence of mesh refinement on the flame wrinkling factor is presented. The coarser mesh gives origin to an earlier increase of the flame wrinkling factor, which then causes the turbulent flame speed to increase. This is the reason for the earlier build-up of heat release speed and the higher cylinder pressure.
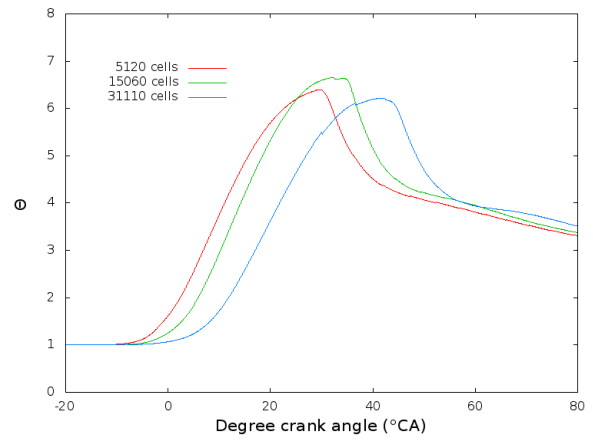
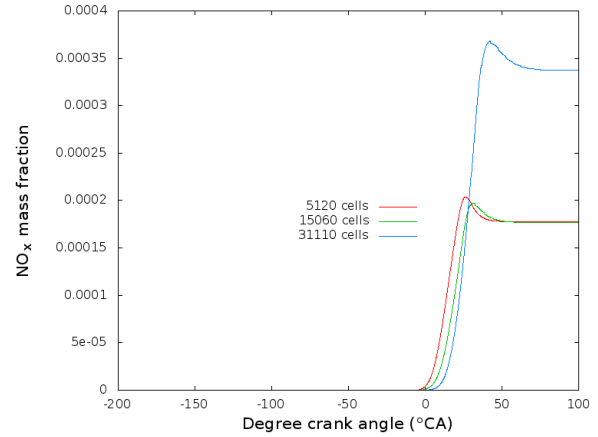

Figure 9. The number of cells influences cylinder temperature

Figure 10. The number of cells influences turbulent kinetic energy

In Figure 12., the influence of the mesh on the NO_x concentration is shown. It can be seen, the characte-ristic pattern of NO_x formation during the most inten-sive combustion period and a small decrease after which

the concentration remains constant. It is surprising that the finest mesh gives origin to the greatest, and much higher concentration of NO_x. The obtained NO_x con-centration cannot be used for absolute formed NO_x quantities evaluation, but the trends in various influen-tial factors can be applied.
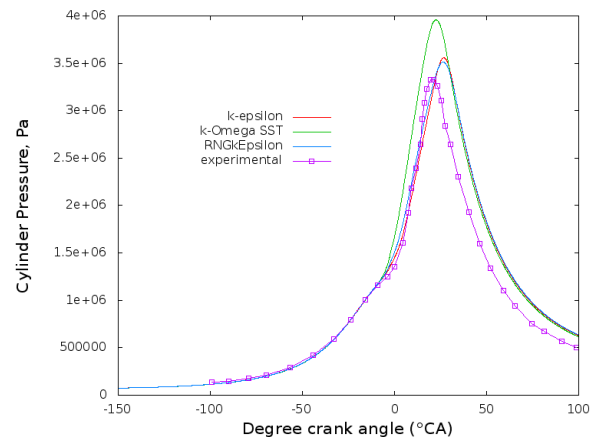

**Figure 11. The number of cells influences the flame wrinkling factor**

Figure 12. The number of cells influences the NO_x mass fraction

4.3 Turbulence model

Here, a preliminary test of the described turbulence mo-dels is performed. The initial parameters were: $k=3$ m^2/s^2 for all the cases and $\varepsilon = 250$ m^2/s^3 for both the k-ε variants and $\omega=5$ s^{-1} for the SST k-ω case.
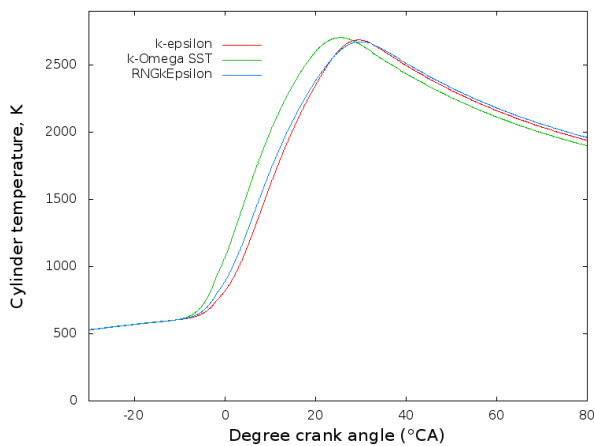

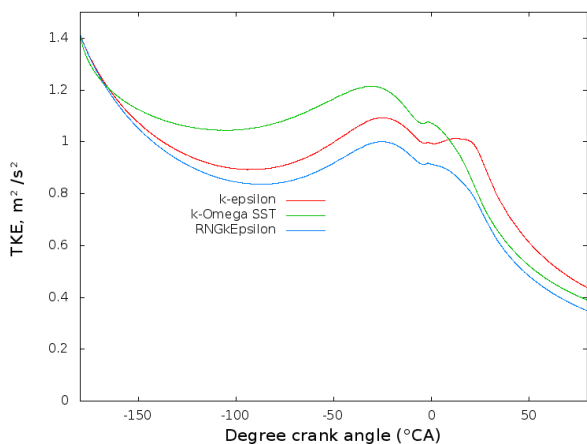**Figure 13. Turbulence model influence on cylinder pressure**
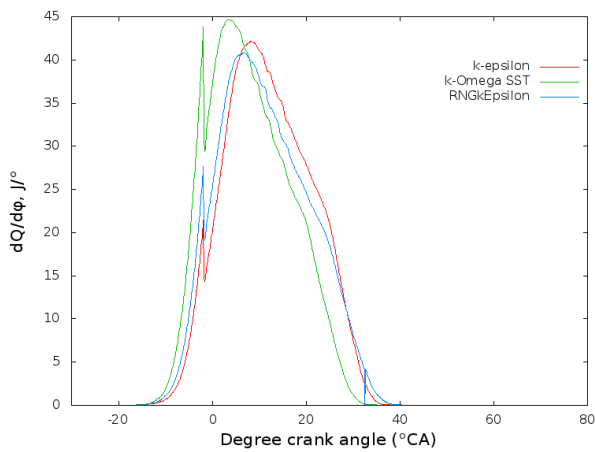
Figure 14. Turbulence model influence on the rate of heat release

Figure 13. shows that the k-ε models (standard and RNG) predict cylinder pressure better while the k-ω SST tends to over-predict it since pressure rise starts earlier than for the measured case. This is the result of an earlier start and more intensive heat release obtained with the k-ω model, Figure 14. This behavior is reflected also by cylinder temperature, Figure 15.
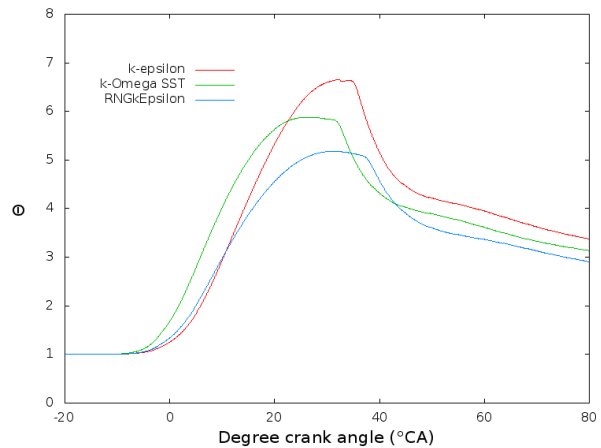

Figure 15. Turbulence model influence on cylinder temperature

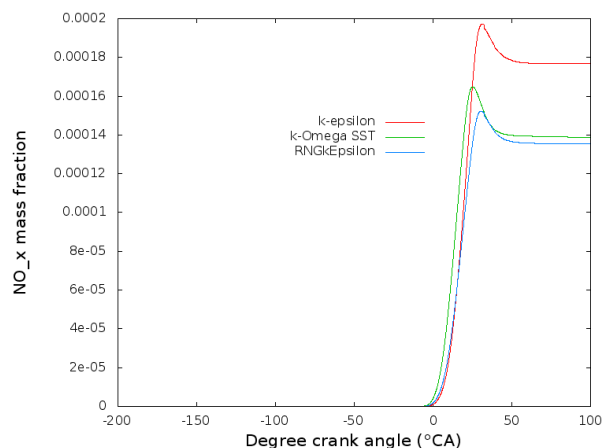**Figure 16. Turbulence model influence on turbulent kinetic energy**

The turbulence model influences directly the level of turbulent kinetic energy, Figure 16. It can be seen that the used k-ω SST dissipates less the turbulent kinetic

energy in the compression phase which leads to higher levels of turbulence during combustion.
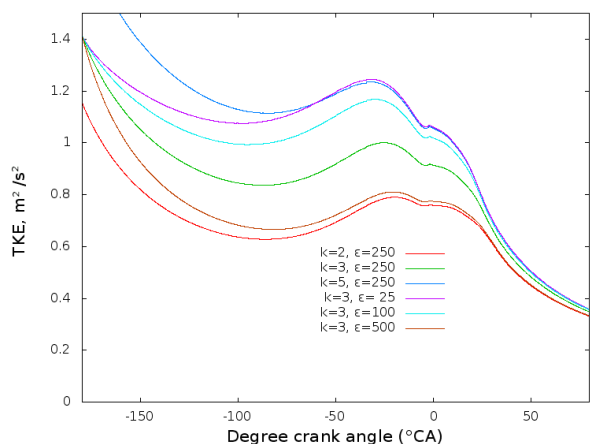

Figure 17. Turbulence model influence on flame wrinkling factor

The flame wrinkling factor is directly influenced by turbulence, Figure 17. While the k-ω SST model causes an earlier rise of Θ, the highest levels are obtained with the standard k-ε model. Very interesting is the influence of the used turbulence model on NO_x concentration, Figure 18. While the k-ω SST and RNG k-ε result in similar NO_x concentrations, the standard k-ε results in a roughly 30% higher final value.

Figure 18. Turbulence model influence on NO_x mass fraction

Figure 19. Initial k and ε influence on the turbulent kinetic energy

4.4 Turbulence model initial values *k* and *ε*

Generally, engine CFD simulations are performed for various sizes and types of engines. Different calculation meshes are used and also different sub-models. The level of turbulent kinetic energy in the cylinder directly influences the flame speed propagation, which is res–ponsible for pressure and temperature build-up and hence also for pollutant formation. The level of cylinder turbulent kinetic energy is not readily measured, hence it is not simple to choose the initial values for the turbulence model. In the OpenFOAM engineFoam sol–ver tutorial named KivaTest, initial $k = 4$, and initial $\varepsilon = 450$ are used while in [6] initial $k = 2.661$ and initial $\varepsilon = 25.763$ are used. [8] used $k = 4$ and $\varepsilon = 450$ for the engine at the speed of 8000 rpm. Here, an attempt to analyze the influence of the turbulence model's initial values is performed. The level of turbulent kinetic energy, *k*, was varied from 2 to 5 m^2/s^2, and the amount of the turbulent kinetic energy dissipation rate ε was varied from 25 to 500 m^2/s^3.

In Figure 19. the cylinder's turbulent kinetic energy is shown. It can be seen that both *k* and *ε* have an important influence on turbulence levels. The highest levels of turbulence are found for the case with an ave–rage initial level ($k = 3$), but a low TKE dissipation rate of $\varepsilon = 25$, and for the high initial turbulence ($k = 5$) case. Lower than average turbulence levels during the process are found for low initial turbulence ($k = 2$) or high turbulent energy dissipation rate cases ($\varepsilon = 500$). This is clearly reflected in the following figure, Figure 20. which shows the flame wrinkling factor Θ.

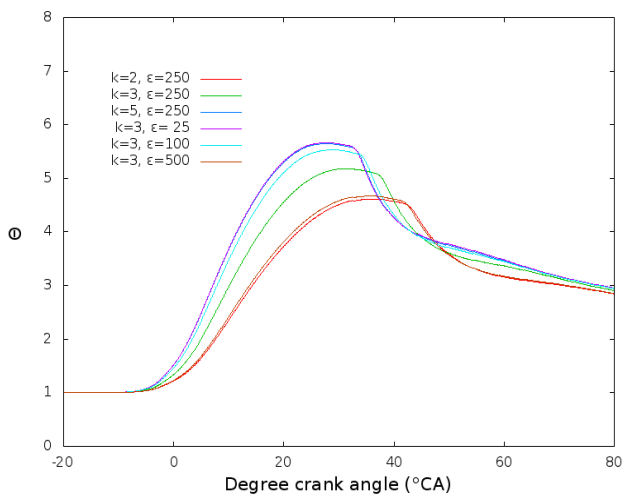**Figure 20. Initial *k* and *ε* influence on flame wrinkling factor**

The cases with higher turbulence levels are from Figure 19. result in higher wrinkling factors. In Figure 21. it can be seen that the higher wrinkling factor leads to faster heat release rates d*Q*/d*φ*.

In Figure 22. the cy–linder pressure is presented. The calculated results can be compared with the experimentally obtained ones. It can be concluded that the case for average initial values of $k = 3$ and $\varepsilon = 250$ result in cylinder pressure levels that are close to those of the experimental pressure. Besides pressure, the heat release rate is reflected in the cylinder's average temperature, Figure 23.
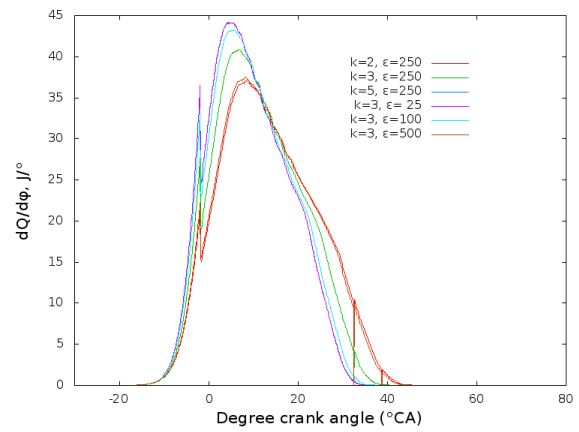

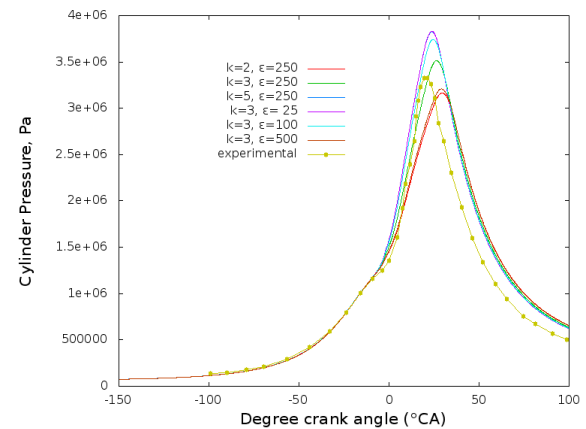**Figure 21. Initial *k* and *ε* influence on the rate of heat release**

Figure 22. Initial *k* and *ε* influence on cylinder pressure
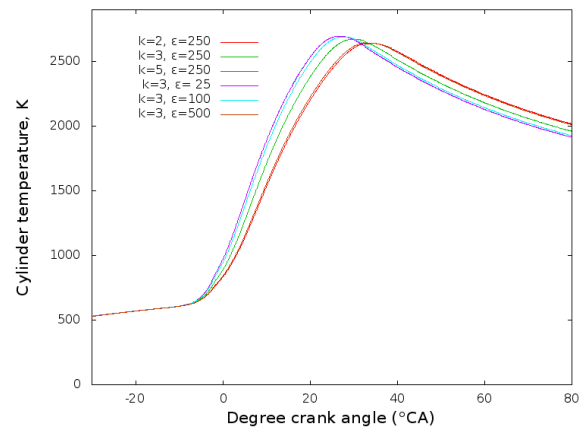
Figure 23. Initial *k* and *ε* influence on cylinder temperature

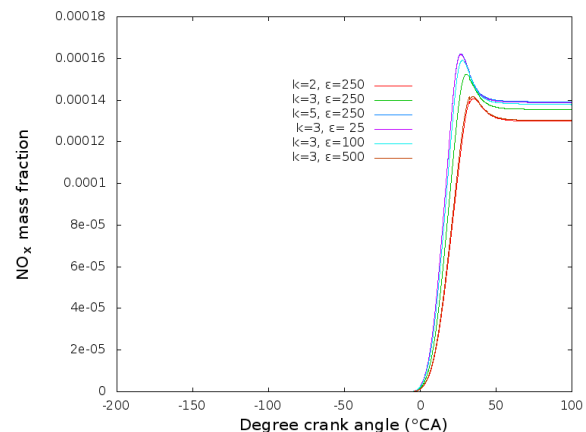**Figure 24. Initial *k* and *ε* influence on NO$_x$ mass fraction**

The maximal temperature reached is very similar for all the cases. The cases with higher turbulence level results in an earlier temperature build-up, and slightly higher temperatures. The temperature is the main influential factor for the NO_x concentration. In Figure 24. it can be seen that the higher temperatures of the cases with higher cylinder turbulence levels result in higher NO_x concentration.

4.5 Combustion model parameters *u'* and Θ

Engine power, efficiency, and emissions performance are highly dependent on the combustion rate. The combustion rate depends on temperature, pressure, mixture compo–sition, and other parameters. In the simulation, the com–bustion rate is modeled as described in the mathematical model. Among other parameters, *u'* and Θ_{coef} are the most influential model parameters. Here, an attempt to gain an insight into the nature of their influence is performed. *u'* was varied from 0.5 to 2.4 and Θ_{coef} from 0.1 to 1. Figure 25. shows the direct influence of the varied parameters on the flame wrinkling factor Θ. The highest values of Θ are reached for the largest value of *u'*=2.4 which raises the flame speed earlier than in other cases. Then the combination of $u' = 1$ and $\Theta_{coef} = 1$ rises the Θ value sensibly almost to the value of 10.

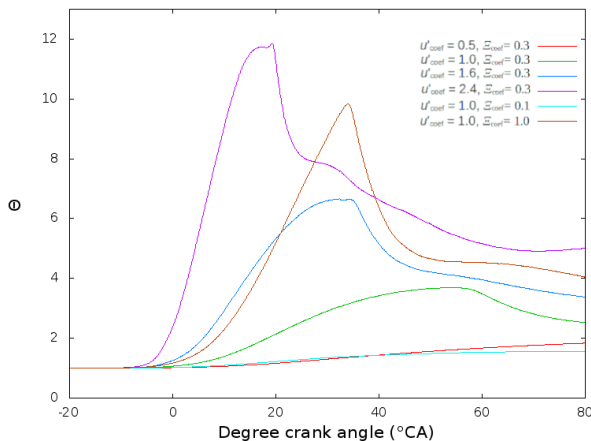**Figure 25.** *u'* and Θ$_{coef}$ influence on the flame wrinkling factor

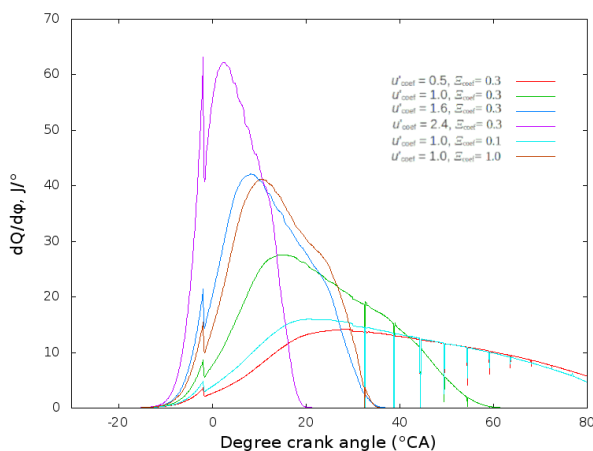**Figure 26.** *u'* and Θ$_{coef}$ influence on the rate of heat release

On the other hand, the Θ value shows a very low and late increase from the initial value of 1 for the combination

of small values of *u'* and Θ_{coef}. In Figure 26. the influence of the flame wrinkling factor Θ on the heat release rate is presented. It can be seen that the combustion speed is greatest for the case with $u' = 2.4$ and $\Theta_{coef} = 1.6$. The combination of *u'*=1 and $\Theta_{coef} = 1$ gives also a relatively fast combustion, while other combinations of parameters lead to a late and slow combustion result. The same trends are reflected also in Figure 27. which shows the cylinder pressure with the experimentally obtained result. It can be observed that the high value of $u' = 2.4$ leads to an overestimation of cylinder pressure. Very good results are obtained for the intermediate values of $u' = 1.6$ with $\Theta_{coef}= 0.3$ and $u' = 1$ with $\Theta_{coef}=1$. For lower values of the model coefficients, the cylinder pressure results are too low. In Figure 28., the influence of the combustion parameters on the turbulent kinetic energy is presented. It can be seen that it rises proportionally more for the combinations of parameters that lead to more intensive combustion.
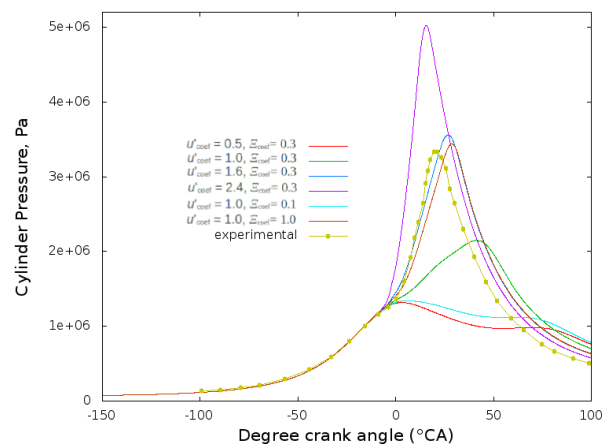

Figure 27. *u'* and Θ$_{coef}$ influence on cylinder pressure
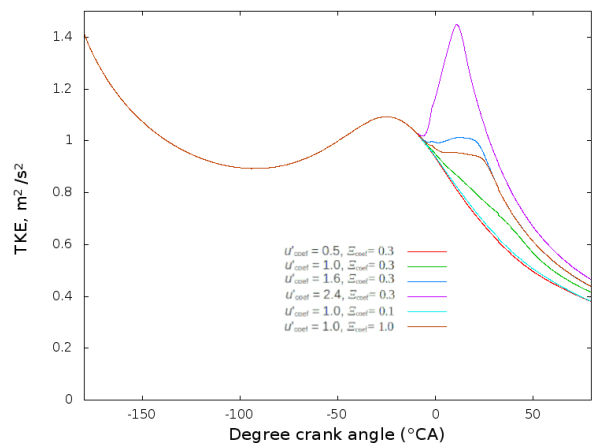
Figure 28. *u'* and Θ$_{coef}$ influence on the turbulent kinetic energy

In Figure 29. the influence of the flame wrinkling parameters on the cylinder temperature are shown. It can be seen that the parameters that increase the flame wrinkling mostly lead to higher temperatures and earlier temperature peaks. The calculated concentration of NO_x is reported in Figure 30. It can be seen that the highest concentration by far is obtained for the case with $u' = 1$ and $\Theta_{coef} = 1$. As expected, for the cases that resulted in low cylinder temperatures, NO_x concentrations are the lowest. The final NO_x concentration is lower for the

highest temperature case ($u' = 2.4$, $\Theta_{coef} = 0.3$) than for the case that underestimated the cylinder pressure and temperature ($u' = 1$, $\Theta_{coef} = 0.3$).

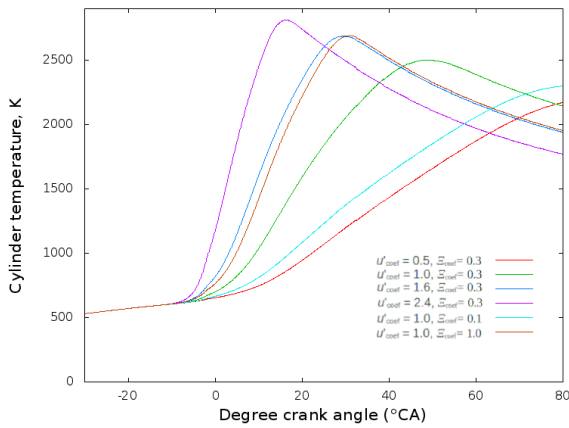**Figure 29.** u' and Θ_{coef} influence on cylinder temperature

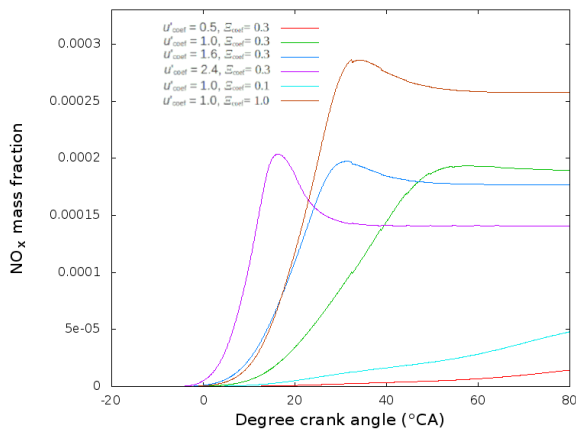**Figure 30.** u' and Θ_{coef} influence on NO_x mass fraction
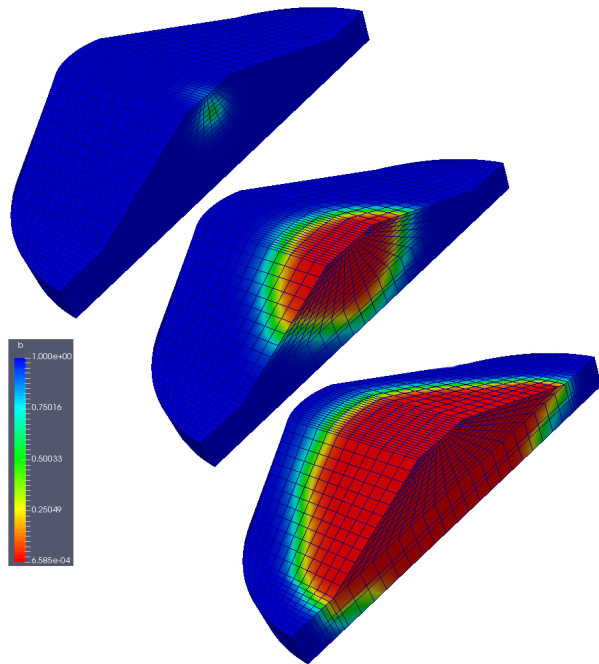

Figure 31. The propagation of the flame regression variable *b* at the moments of -10, 0, and 10 °CA

In Figure 31. a graphical presentation of the flame propagation in the cylinder with time is presented. Speci-fically, the regression variable b is presented for the moments of -10, 0, and 10 °CA.

5. CONCLUSION

In the present paper, the basic parameters of a CFD simulation of a spark ignition, internal combustion en-gine are analyzed.

The simulation mesh that reproduces half of the do-main resulted in the best compromise for accuracy, simplicity, and calculation time. The simpler meshes, a 2D and a 1/4 sector mesh showed excessively fast or slow combustion compared to the experimental results. The more complex, full 3D mesh did not behave better than the half mesh, it was more complex to build and lead to a slower calculation.

By increasing the mesh refinement (number of cells in the domain, smaller cells) with fixed all other parameters, the flame propagation speed is dampened. Hence, heat release rate and maximum pressure, and temperature are decreased. The influence on the turbulence kinetic energy and the flame wrinkling factor is smaller and not so direct. The implemented NOx model is sensitive to mesh refine-ment and resulted in a big increase in concentration for the finest mesh tested. The mesh that yields 15060 cells at the beginning and 5220 cells around TDC was selected as the best compromise for this size of the engine.

The RNG k-ε model showed to be the most approp-riate. The tested k-ω over estimated cylinder peak pressure while the standard k-ε resulted in excessive NOx produc-tion. Clearly, it is possible that the results could be tuned by choosing different initial values for turbulence and turbulence dissipation, or different model parameters. The initial parameters influence was investigated for the RNG k-ε model. The turbulence level is recalculated after the internal velocity conditions, but initial values do influence all the other observed parameters. The turbulence kinetic energy can be reduced by choosing a low initial value or a high initial value of turbulent kinetic energy dissipation. The best results are obtained for the case with initial values of k =3 and ε=250. The influence of the turbulence model's initial parameters on NOx emissions is low. Finally, the influence of the flame wrinkling model parameters u' and Xi$_{coef}$ are tested. They can be used to tune the flame speed to a certain level. The heat release rate can be boosted by increasing any of the two coefficients. Best results are obtained for the combination of u' = 1.6 and Xi$_{coef}$ = 0.3. The case with 1 for both the parameters gave also very good results, but unexpectedly raised a lot the concen-tration of calculated NOx.

The simple extended Zeldovich-based NOx model re-sults in concentrations of the same order of magnitude as in other similar investigations. It is known that it can be tuned with different model coefficients, but that is not the point. It can be used to observe the influence that some working parameters of the engine have on the final NOx emissions.

An overview of the main initial parameters of common spark ignition engines is performed. It is shown that various different parameters in a CFD simulation model can be adjusted to obtain a numerical result as close as possible to the measured one. The results and conclusions obtained in this analysis will be used as a baseline for

further simulations of various piston engines with different fuels and combustion models.

REFERENCES

[1] Jasak, H., Jemcov, A., Tuković, Ž.: OpenFOAM: A C++ Library for Complex Physics Simulations, International Workshop on Coupled Methods in Numerical Dynamics, Dubrovnik, Croatia, 2007

[2] Jasak, H.: OpenFOAM: open source CFD in research and industry, International Journal of Naval Architecture and Ocean Engineering, Vol. 1(2), 2009

[3] Jasak, H.; Weller, H.; Nordin, N.: In-Cylinder CFD Simulation Using a C++ Object-Oriented Toolkit; SAE Technical Paper 2004-01-0110; SAE Mobilus: Washington, DC, USA, 2004

[4] Amirante, R., Distaso, E., Tamburrano, P., Reitz, R.D Laminar flame speed correlations for methane, ethane, propane and their mixtures, and natural gas and gasoline for spark-ignition engine simulations, International J of Engine Research 2017, Vol. 18(9) 951–970, DOI: 10.1177/1468087417720018.

[5] Chatakonda, O, Hawkes, E. R., Brear, M. J., Chen J. H., Knudsen E., Pitsch, H.: Modeling of the wrinkling of premixed turbulent flames in the thin reaction zones regime for large eddy simulation, Center for Turbulence Research, Proceedings of the Summer Program, 2010

[6] Anetor, L., Edward, E. O., Kendall, H.: Simulation Studies of Combustion in Spark Ignition Engine using Openfoam, FME Transactions (2020) 48, 787-799, doi: 10.5937/fme2004787A

[7] Sendyka, B., Noga, M.: Combustion Process in the Spark-Ignition Engine with Dual-Injection System, Advances in Internal Combustion Engines and Fuel, 2013, Technologies, DOI: 10.5772/54160

[8] Gundmalm, S.: CFD modeling of a four stroke S.I. engine for motorcycle application, Master of Science Thesis, Stockholm, Sweden 2009

[9] Battistoni, M., Mariani, F., Risi, F., Poggiani, C.: Combustion CFD modeling of a spark ignited optical access engine fueled with gasoline and ethanol, Energy Procedia 82 (2015), 424–431

[10] Mashkour, M. A., Ibraheem, M. H.: Numerical Simulation of pent-roof combustion chamber in a SI Engine, Journal of Mechanical Engineering Research and Developments, Vol. 43, No. 7, pp. 422-433, 2020.

[11] Yin, C., Zhang, Z., Sun, Y., Sun T., Zhang, R.: Effect of the piston top contour on the tumble flow and combustion features of a GDI engine with a CMCV: a CFD study, Engineering Applications of Computational Fluid Mechanics, 10:1, 311-329, 2016, DOI: 10.1080/19942060.2016.1157099

[12] Mauro, S., Şener, R., Gül, M.Z., Lanzafame, R., Messina, M., Brusca, S.: Internal combustion engine heat release calculation using single-zone and CFD 3D numerical models, International Journal of Energy and Environmental Engineering, 2018., https://doi.org/10.1007/s40095-018-0265-9

[13] Kutkan, H., Guerrero, J.: Turbulent Premixed Flame Modeling Using the Algebraic Flame Surface Wrinkling Model: A Comparative Study between OpenFOAM and Ansys Fluent, Fluids 2021, 6, 462.

[14] Joshi, A., Borse, S. L., Alblawi, A., Alshqirate A. A.: Effect of spark plug position of n performance of engine using OpenFOAM, International Journal of Mechanical Engineering and Technology (IJMET), Volume 9, Issue 11, November 2018, pp. 114–120

[15] Spalding, D.B.: Mixing and chemical reaction in steady confined turbulent flames., Thirteenth Symposium on Combustion, pp. 649 –657, The Combustion Institute, Pittsburgh, PA, 1970.

[16] Cant, R.S., Bray, K. N. C.: Strained Laminar Flamelet Calculations of Premixed Turbulent

Combustion in a Closed Vessel, Twenty-Second Symposium on Combustion, The Combustion Institute, pp. 791-799, 1990.

[17] Masuya, G., Influence of Laminar Flame Speed on Turbulent Premixed Combustion, Combustion and Flame, 64, 1986

[18] Weller, H. G., Tabor, G., Gosman, A. D., Fureby, C.: Application of a Flame-Wrinkling LES Combustion Model to a Turbulent Mixing Layer, Twenty-Seventh Symposium on Combustion, The Combustion Institute, pp. 899–907, 1998.

[19] Yakhot, V., Orszag, S. A., Thangam, S., Gatski, T. B., Speziale, C. G.: Development of turbulence models for shear flows by a double expansion technique, Physics of Fluids A, Vol. 4, No. 7, 1992

[20] Wilcox, D. C.: Formulation of the k-ω Turbulence Model Revisited, AIAA Journal, Vol. 46, No. 11, 2008, doi:10.2514/1.36514

[21] Zeldovich, Y. A.: The Oxidation of Nitrogen in Combustion and Explosions, Acta Physicochim. URSS 21: 577-628, 1946.

[22] Murić, K.: Modeling of NOx formation in heavy duty engines, Master Thesis, Lund University, 2011

[23] Lucchini, T., D'Errico, G., Jasak, H., Tukovic, Z.: Automatic mesh motion with topological changes for engine simulation (2007) SAE Technical Papers

[24] Senčić, T., Mrzljak, V, Blecich, P., Bonefačić, I: 2D CFD Simulation of Water Injection Strategies in a Large Marine Engine, Journal of Marine Science and Engineering, Vol **7** (2019), 9; 296, 18 doi:10.3390/jmse7090296

NOMENCLATURE

b	Flame regression variable
e	Specific internal energy
g	Specific body force
J	Heat flux vector
k	Turbulent kinetic energy
p	Pressure
R	Gas constant
R_η	Kolmogorov Reynolds number
S_{ct}	Turbulent Schmidt number

S_t	Turbulent flame speed
S_{ub}	Laminar flame speed
t	Time
T	Temperature
u	Gas velocity vector
u'	Subgrid turbulence intensity
Q^c	Source term due to chemical heat release

Greek symbols

ρ	Density
σ	Viscous stress tensor
Θ	Flame wrinkling factor
ε	Turbulent kinetic energy dissipation rate
ω	The specific rate of dissipation of the turbulent kinetic energy into internal thermal energy
μ_t	Turbulent viscosity

List of acronyms

2D	Two - Dimensional
3D	Tri - Dimensional
BDC	Bottom Dead Course
CA	Crank Angle
CFD	Computational Fluid Dynamics
CFR	Cooperative Fuel Research
CMCV	Charge motion control valve
FOAM	Field Operation And Manipulation
GDI	Gasoline Direct Injection
HCCI	Homogeneous Charge Compression Ignition
IC	Internal Combustion
RNG	Re-Normalization Group

SST	Shear Stress Transport
TDC	Top Dead Course

УТИЦАЈ ПАРАМЕТАРА МРЕЖЕ И САГОРЕВАЊА НА CFD СИМУЛАЦИЈУ МОТОРА СА ВАРНИЧКИМ ПАЉЕЊЕМ

Т. Сенчић, В. Мрзљак, О. Буковац, Ј. Батиста

У овом раду је спроведена студија симулације CFD-а на мотору са косим кровом, са паљењем свећом. Циљ је био да се анализирају основни параметри који утичу на перформансе симулације: конфи–гурација мреже, пречишћавање мреже, модел турбу–ленције и параметри модела набора пламена. Кори–шћен је као OpenFOAM решавач за моторе са вар–ничним паљењем. Решавач је модификован дода–вањем механизма за додавање/уклањање слојева за мрежу. Надаље, имплементиран је Зелдовицх про–ширени NOx модел. Тестиране су четири различите конфигурације мреже са различитим нивоима префињености. Тестиран је скуп различитих модела турбуленције и почетних параметара и различитих параметара модела наборања пламена. Уочено је како сви ови параметри утичу на брзину ослобађања топлоте, притисак у цилиндру, температуру, ниво турбулентне кинетичке енергије, фактор наборања пламена и коначно на резултујућу концентрацију нитрид моноксида.